Journal of Alloys and Compounds 786 (2019) 84–90

Contents lists available at ScienceDirect

Journal of Alloys and Compounds

journal homepage: http://www.elsevier.com/locate/jalcom

Transport properties of resistive switching in $Ag/Pr_{0.6}Ca_{0.4}MnO_3/Al$ thin film structures

V. Lähteenlahti*, A. Schulman, H. Huhtinen, P. Paturi

Wihuri Physical Laboratory, Department of Physics and Astronomy, University of Turku, FI-20014 Turku, Finland

ARTICLE INFO

Article history:
Received 10 October 2018
Received in revised form
21 January 2019
Accepted 24 January 2019
Available online 30 January 2019

Keywords:
Resistive switching
Perovskite oxides
Switching mechanics
PCMO
Memristor
Neuromorphic

ABSTRACT

Thin films of $Pr_{0.6}Ca_{0.4}MnO_3$ were prepared by pulsed laser deposition with an asymmetric pair of Ag and Al metal electrodes in order to study their resistive switching properties. The devices exhibited stable voltage controlled bipolar switching which proved to be reliable and non-volatile. The resistive states show a well-defined dependence on the write voltage, which was used to achieve several intermediate states, indicating that the devices could be utilized in hardware implementations of neuromorphic computing. The switching mechanism was attributed to the electric-field assisted migration of oxygen vacancies at the Al-electrode interface, resulting in a formation and modulation of a rectifying interfacial AlO_x layer. The current-voltage characteristics were analyzed by means of the power exponent representation, which hinted to a device state dependent interplay of bulk-limited Poole-Frenkel conduction and interface-limited Schottky conduction. A deeper understanding of resistive switching characteristics in $Ag/Pr_{0.6}Ca_{0.4}MnO_3/Al$ will lead towards further advances in manganite-based neuromorphic circuits.

1. Introduction

Present day's computers suffer from the von Neumann bottleneck, in which the processing speed is limited by the bus which connects memory and the central processing unit [1]. Neuromorphic computer architectures show a possible way to bypass this limit since they do not divide memory and computations into separate units, which enables highly parallel computations [2–4]. In possible hardware implementations of neuromorphic computing, devices that behave more similarly to biological synapses and neurons are preferable over the traditional CMOS (complementary metal-oxide-semiconductor) solutions, which are not efficient for these tasks since the technology was designed for a different purpose [5,6].

The implementation of these new technologies will require the utilization of new and more efficient materials. In particular, metal oxides, which have gained a lot of attention for their rich chemical and physical properties and versatile applicability in many areas, such as energy storage, solar cells and sensors [7–14]. Metal oxides have also found their place in resistive switching (RS) devices [15,16]. Due to the RS property present in many metal oxides, they now present a notable portion of promising memristive materials [17].

Oxide based resistive switching devices are suitable for mimicking neurons and storing synaptic weights [18–23]. Indeed, neuromorphic circuits containing RS elements are starting to show promising results, particularly in the field of spiking neural networks, where the RS oxide can reproduce dynamics found in biological systems with minimal amount of additional circuitry [24]. However, more research is still needed to understand the physics behind the RS in order to maximize the capabilities of these systems [25,26].

Among the oxides which present the RS behavior, the perovskite oxide $Pr_{1-x}Ca_xMnO_3$ has been proven to be versatile, exhibiting both bipolar [22] and unipolar [27] switching with and without forming [28,29]. The interface-type bipolar switching in particular has been found useful in neuromorphic applications, which has led to PCMO-based implementations of single neurons as well as neuromorphic arrays [26,30–32].

Even though the RS in $Pr_{1-x}Ca_xMnO_3$ has been extensively studied [17,28,29,33–38], new ways to improve the switching properties are still being found by the means of interface engineering with buffer layers and oxygen treatments [22,39]. In addition, the core of the work on RS in PCMO has been performed with $x = 0.3$, although it has been shown that other concentrations can result in better RS properties [36]. The conduction model of

* Corresponding author.
E-mail address: visalah@utu.fi (V. Lähteenlahti).

https://doi.org/10.1016/j.jallcom.2019.01.279

bipolar switching has also been usually attributed to the trap-controlled space-charge-limited current (SCLC) conduction [33,38,40–44] with exponentially distributed traps, although the use of a more in depth analysis method [45] gives an alternative explanation. Thus improving the understanding of RS and conduction mechanisms in PCMO is still possible and a remains as a path towards realization of more robust neuromorphic devices.

In this work we studied the RS characteristics of $Pr_{1-x}Ca_xMnO_3$ with an optimal concentration of $x = 0.4$, hereafter labeled PCMO. In PCMO, the bipolar switching is determined by the interfaces [28]. Due to this, we studied the interface properties of Metal/PCMO/Metal structures with different metallic electrode combinations. The utilized metals were Ag, Au and Al, of which we found that only the Al interface produces a strong bipolar RS effect. The switching attained by using Al/PCMO/Ag interfaces exhibits multiple states and was both reliable and non-volatile. The cause of the switching is attributed to oxygen vacancy migration at the Al/PCMO interface. The conduction model is analyzed, hinting to an interplay of bulk-limited PF conduction and interface-limited Schottky conduction depending on the device state and polarity of the electric field.

2. Experimental details

$Pr_{0.6}Ca_{0.4}MnO_3$ thin films with thicknesses of approximately 100 nm were deposited on $5 \times 5 \times 0.5$ mm^3 (100) $SrTiO_3$ substrates by pulsed laser deposition (PLD) using excimer XeCl 308 nm laser. The pulse duration was 25 ns, repetition rate 5 Hz, laser fluence 1.3 J/cm^2 and the pressure of flowing oxygen in the chamber 0.175 torr. The films were grown at a temperature of 500°C, with *in situ* post-annealing treatment of 10 min in atmospheric oxygen pressure. The used rate for cooling and heating was 25°C/min. The grown films were verified to be well-crystallized and epitaxially textured by X-ray diffraction (Fig. 1a) with lattice parameters $a = 5.4354$ Å, $b = 7.6511$ Å and $c = 5.4277$ Å. More details on the growth process can be found in Ref. [46].

0.5 mm diameter Au and Ag metal contacts were deposited on top of the films using room-temperature Ar-ion sputtering. Wiring was done with a wedge bonder using a 40 μm diameter Al-wire. Measurements were performed in a planar configuration as schematized in the inset of Fig. 1c using a Keithley 2614b source/measure unit. The separation distance between the electrodes was approximately 200 μm.

Loop measurements of electrical characteristics were done at room temperature by sweeping the voltage in a sequence of steps $0 \rightarrow V_{max} \rightarrow -V_{min} \rightarrow 0$ with logarithmic amplitude progression, 10 ms step width and a 10 ms low-voltage read between each step. Multiple films were studied, and the characteristics were found to be consistent between the samples.

All combinations of Al, Ag and Au Metal/PCMO/Metal interfaces were measured, and only combinations containing Al were found to produce switching. Both Ag and Au interfaces formed a linear Ohmic contact with PCMO (Fig. 1b), and thus didn't contribute to the switching. When Al interface was present, the conduction was non-linear.

Since the work function of p-type [36] $Pr_{0.6}Ca_{0.4}MnO_3$ is close to values reported for other concentrations: $\phi \approx 4.9$ eV [47] for $x = 0.3$ and $\phi \approx 4.8$ eV for $x = 0.5$ [36], a more rectifying interface is expected for the Al ($\phi = 4.06–4.26$ eV [48]) than for the Ag ($\phi = 4.26–4.47$ eV [48]) due to the differences in work functions, which is in agreement with the measurements (Fig. 1b).

In the case of Al/PCMO/Al, the conduction reproduced the "table-with-legs" profile (Fig. 1b), which has previously been obtained by simulating dielectric with a changing oxygen vacancy profile between two electrodes [49]. The presence of the table-with-legs shape indicates that both of the Al interfaces are active in switching, and introducing asymmetry in the electrodes will enhance the bipolar switching properties.

When asymmetry was introduced into the electrodes by using Au/PCMO/Al or Ag/PCMO/Al (Fig. 1b) the RS properties were greatly increased as predicted by the simulations. Thus we selected the combination of rectifying Al and Ohmic Ag interfaces for further studies. The combination ensures us that the RS is dominated by the Al/PCMO interface and only one of the two interfaces is active in switching.

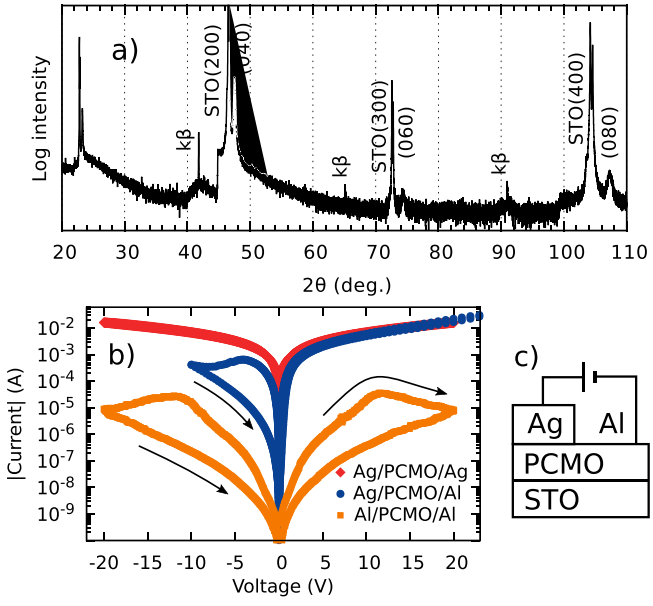

Fig. 1. a) XRD diffractogram of (lkl) peaks. b) I-V loops for PCMO with combinations of Ag and Al interfaces, symmetrical Ag-interfaces show Ohmic conduction, while interfaces containing Al show non-linear conduction and rectifying behavior. c) Measurement geometry.

3. Results and discussion

3.1. Bistable switching

A typical example of a stable bipolar switching is presented in Fig. 2. The device can be switched between HRS (high resistance state) and LRS (low resistance state) in a closed loop by applying positive and negative voltage sweeps. Negative polarity induces the

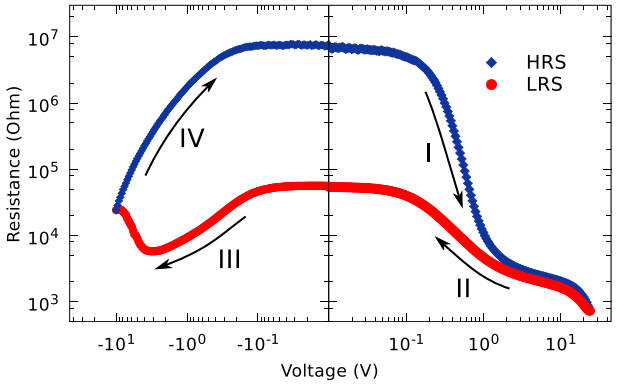

Fig. 2. A single bipolar switching loop showing device resistance as a function of applied voltage. Positive polarity induces the LRS while the negative polarity resets device into the HRS.

transition to HRS and positive to LRS. The resistance of a pristine device is initially between the HRS and LRS resistances and doesn't need electroforming in the conventional sense, although the first loops show irregular step changes. Similar forming-free behavior has been observed for both bipolar and unipolar switching in PCMO and has been found to be affected by both electrode materials and growth conditions [28,29]. As there is no high-voltage forming process or current limitation involved, the device homogeneity is good and the devices show predictable behavior with similar resistance values across different samples. The HRS and LRS voltages were chosen to obtain a reasonable compromise between a high switching ratio and reliability. The voltages needed for switching could be further reduced by miniaturizing the device dimensions. It is worth noting that no switching is observed if the applied voltage is below certain threshold which for our geometry is $V_{th} = 3$ V. This is of great importance since neuromorphic devices require a possibility of non-destructive reading of the resistive state.

We didn't notice any variation in the behavior of the devices when changing the electrode separation distance, indicating that the dominant switching effect is not caused by filamentary conduction paths. The measurements rule out the involvement of Ag-ions, as well as intrinsic switching PCMO bulk, since it has been shown that the bulk PCMO switches with unipolar behavior [29]. This leaves oxygen vacancy movement near the interface region as the main culprit for changes in conductivity.

Within the generally accepted framework for the origin of the RS in oxides [27,36,49–52], the bipolar switching is attributed to the electric field assisted migration of oxygen vacancies [49] near the Al/PCMO interface. Due to differences in the oxidation energies when the devices are in the pristine state, an oxide layer is formed at the interface, generating a Schottky-like barrier [35].

Passing a current through the device produces a large electric field at the interface due to the high resistivity of the barrier. The electric field enables movement of oxygen vacancies towards or away from the interface, which modulates the oxide layer thickness, resulting in either lowered or increased conductivity across the entire device. The process is reversed by applying an opposite voltage which causes migration of mobile oxygen vacancies to the opposite direction. The effect is limited to the interface due to the lower electric field inside the bulk. In addition, electric transport inside the PCMO bulk is a result of double-exchange interaction, which relies on oxygen atoms, thus introducing more oxygen vacancies decreases the conductivity [53]. Aluminum oxide formation at metal-manganite interfaces has been observed experimentally and changes depending on the RS state [37,54,55].

3.2. Conduction mechanism

In order to better understand the physical origin of the RS, we need to study the conduction mechanism in more detail. For this, we utilize the power exponent representation [45] which allows for a more in-depth determination of the dominant conduction mechanism than the commonly used method where power exponents are obtained by fitting to manually selected regions of interest. The analysis considers a quantity $\gamma = \mathrm{d}(\ln(|\mathrm{I}|))/\mathrm{d}(\ln(|\mathrm{V}|))$ for the whole voltage range, giving power exponents for all the datapoints. Different non-linear (NL) elements [56] produce distinct γ to |V| dependencies, which can be used to differentiate between conduction models. For example, an Ohmic junction ($I \propto V$) will result in a constant $\gamma = 1$, while a SCLC ($I \propto V^2$) dominated interface will have a constant of $\gamma = 2$. Conduction mechanisms that have an exponential dependence between current and voltage, such as Poole-Frenkel (PF) and Schottky, will present a straight line which will only differ in the y-intercept value (0 for Schottky and 1 for PF).

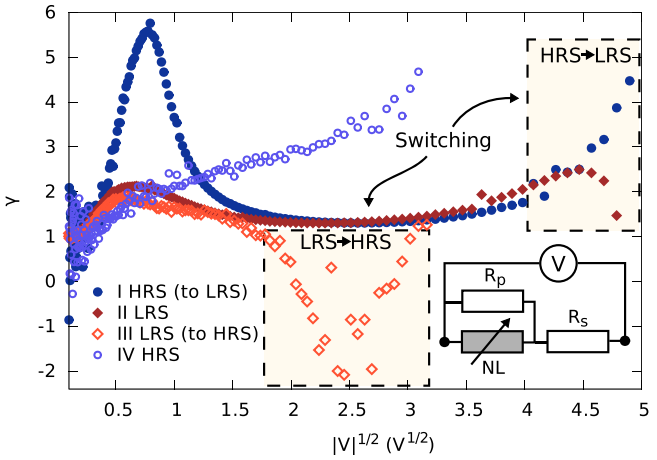

Fig. 3. A $\gamma(V)$ plot where $\gamma = \mathrm{d}(\ln(|\mathrm{I}|))/\mathrm{d}(\ln(|\mathrm{V}|))$, showing the power exponent at each point of the bipolar switching loop of Fig. 2 with the same correspondence between the curves I-IV. The inset shows an equivalent circuit for the system, consisting of a non-linear element (NL) with parallel and series resistances R_p and R_s.

The analysis of the IV characteristics for both the HRS and LRS is presented in Fig. 3. Starting the loop in the HRS and at the positive polarity (curve I) we can distinguish 3 main regions. At low voltages there is a clear Ohmic behavior where γ is 1. At intermediate voltages (200 mV–3 V) there is a peak with a maximum exponent of 6 and then a stabilization to an exponent between 1 and 2. Switching towards the LRS begins at a voltage of around 12 V. Once in the LRS (curve II) the situation is fairly similar, but the peak is less pronounced, with a maximum of 2. The LRS at the negative polarity (curve III) mirrors the positive polarity LRS dependence until the switching to HRS begins at a voltage of 3 V. After the switch from LRS to HRS, the conduction mechanism of the negative polarity changes (curve IV) and the curve resembles a line with an intercept value between 0 and 1.

It is clear that LRS and HRS have different characteristics. On one hand the LRS is symmetrical indicating a bulk-dominated conduction mechanism. On the other hand, the HRS presents rectifying behavior and shows a linear γ-dependence in the curve IV, suggesting that a Schottky-like barrier is dominant in this state. To properly explain the peak shape of $\gamma(V)$, a more complex circuit needs to be introduced. For this we consider an equivalent circuit (Fig. 3) consisting of a switching non-linear element (NL) with Ohmic series and parallel resistances R_s and R_p. The non-linear element (NL) representing the contribution of the Al/PCMO interface can be thought as a bulk-limited PF conduction in series with a Schottky diode [57]. The series resistance R_s represents the contribution from the oxide layer and the parallel resistance R_p the contribution from regions of the interface which do not contribute to the switching.

The resistive switching influences the AlO_x layer, which translates into changing the Schottky barrier of the NL-element [58] and determines whether or not it has a significant contribution to the total conductivity. In the LRS the barrier is thinner and the amount of rectification is reduced. Conversely, in the HRS the barrier is thicker and the interface becomes rectifying. When the NL element is forward biased the PF contribution dominates over the Schottky mechanism and while in the reverse bias the dominating mechanism can be either Schottky or PF depending on the RS state.

Indeed, in the real device the forward biased HRS curve I and both of the LRS state curves II and III have a distinct shape which corresponds to a PF conduction with Ohmic series and parallel resistances R_s and R_p (Fig. 3) and the reverse biased HRS curve IV

resembles rectifying Schottky conduction. Out of the PF-shaped curves the HRS has a higher maximum exponent than the LRS. In terms of the equivalent circuit, this means that in the HRS the ratio of non-linear resistance to parallel resistance R_p is higher, thus we can determine HRS and LRS solely from the $\gamma(V)$ curve shape [45].

3.2.1. Conduction model fitting

By considering a model consisting of a PF-element with series and parallel resistances R_s and R_p we can form an implicit equation for I and V:

$$I = A(V - I{\cdot}R_s)\left[\exp\left(B\sqrt{V - I{\cdot}R_s}\right)\right] + \frac{V - I{\cdot}R_s}{R_p}, \quad (1)$$

with $A = \tilde{A}_{PF}\exp\left(-\frac{q\phi_B}{k_B T}\right)$, $B = \frac{q^{3/2}}{k_B T(\pi\varepsilon_0\varepsilon' d)^{1/2}}$, where T is the temperature, $\tilde{A}_{PF}$ is a constant, q the electron charge, ϕ_B the trap energy level, k_B the Bolzmann constant, ε_0 the vacuum permittivity, ε' the real part of the dielectric constant, d the distance where the voltage drop is produced, R_s the series resistance and R_p the parallel resistance [45].

Table 1
Fit results for parameters A, B, R_p and R_s for HRS and LRS.

State	A (Ω^{-1})	B ($V^{-1/2}$)	R_p (Ω)	R_s (Ω)
HRS	$8.0{\cdot}10^{-10}$	12.87	1923	$6.0{\cdot}10^{6}$
LRS	$1.4{\cdot}10^{-6}$	6.79	1586	$5.0{\cdot}10^{4}$

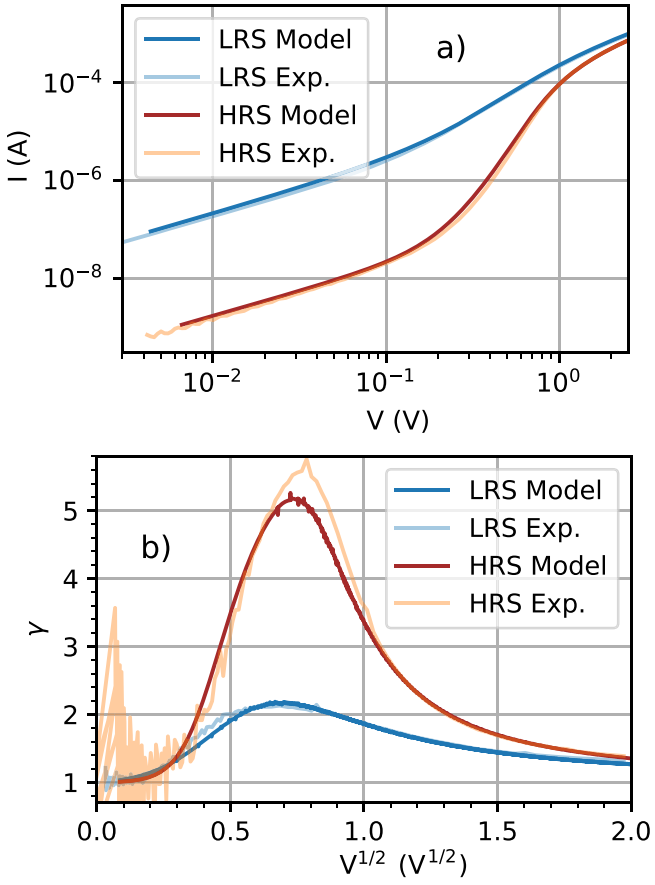

Fig. 4. Comparison between experimental values and a fitted PF conduction model with series and parallel resistances for a) V-I and b) $V^{1/2}$-γ at positive polarity.

Equation (1) has 4 fit parameters A, B, R_s and R_p. By performing a fit to the measured HRS and LRS I-V curves at positive polarity (Table 1) we obtain results which agree with experimental observations and reproduce the γ behavior (Fig. 4). The series resistance values R_s are close to the measured experimental values of $6.8{\cdot}10^{6}$ Ω for HRS and $5.6{\cdot}10^{4}$ Ω for LRS, and the parallel resistance R_p is close to the resistance of 1575 Ω measured from Ohmic Ag/PCMO/Ag interfaces, which corresponds to a situation where the oxide layer R_s and the PF-element are not present. From the parameter A we can qualitatively deduce that the trap energy level ϕ_B is larger in HRS than in the LRS.

The results from the conduction model fitting further reinforce the proposed switching based on an AlO_x interface layer. The changing non-linear interface resistance is associated with the oxide layer at the Al/PCMO-interface. The HRS corresponds to a thicker AlO_x layer with high resistance and an asymmetric contact where the conduction is limited by the Schottky barrier. In the LRS the oxide layer is reduced, weakening the rectifying contact enough to make the symmetric PF conduction dominate.

3.3. State retention and endurance

Since reliability is a very important factor in the design of new electronic elements and a known weakness of the RS-based devices, we analyzed the endurance and state retention of our devices. To do so we utilize a single write pulse protocol with asymmetrical voltages of 18 V and −16 V. The results for repeated alternating HRS and LRS writes are presented in Fig. 5a. The resistance was read with a voltage of −200 mV between the writes. The read voltage was selected to be in the Ohmic region to secure a correct reading of the non-volatile state and to avoid possible accidental writes.

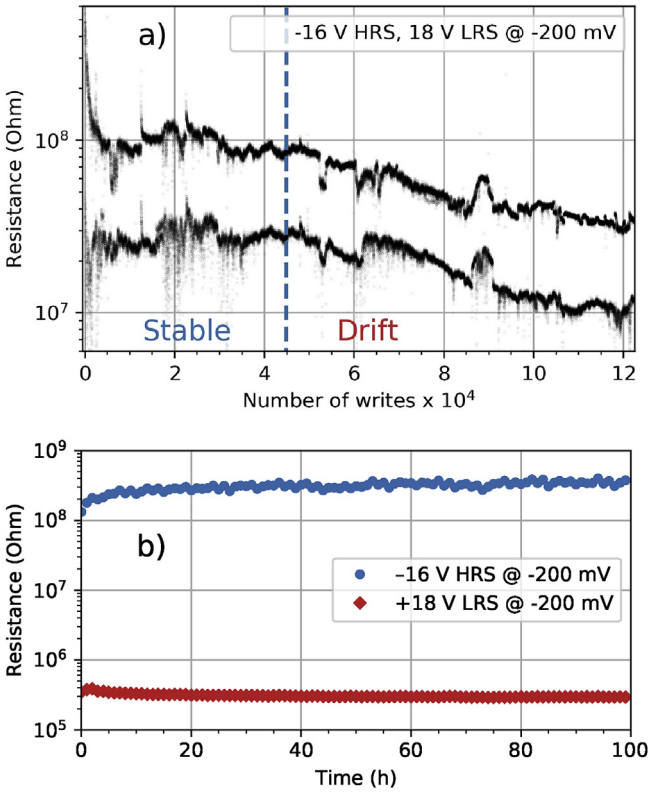

Fig. 5. a) Device resistance over 10^5 repeated writes. b) State retention measurements for HRS and LRS over a timespan of 100 h.

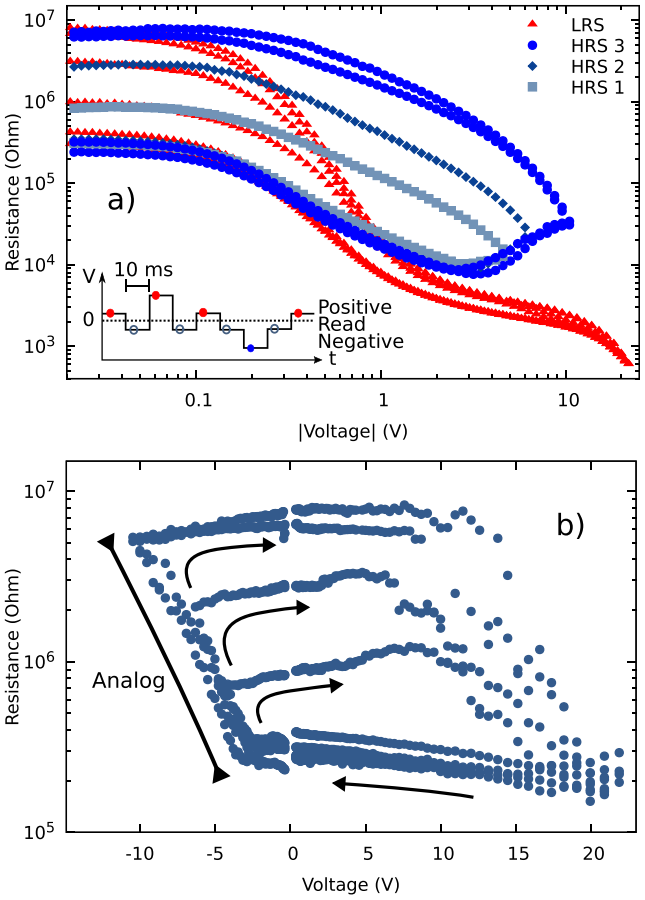

Fig. 6. Multilevel switching showing both a) instantaneous and b) remnant resistances for multiple loops of varying LRS write amplitudes. The remanent resistance shows a well-defined dependence on write voltage on negative polarity.

The endurance tests were done with over 10^5 repeated writes without losing the RS. Initially the device showed large changes in HRS and LRS resistances, after which the switching ratio stabilized. HRS and LRS states stayed distinguishable with respect to the previous state over the whole experiment, although a visible drift towards lower resistances was seen after $5 \cdot 10^4$ writes. The drift was caused by the constant write voltages and has been observed in other RS compounds [59]. The local electric field inside the bulk region is much lower than at the interface, which causes some vacancies to get stuck inside the bulk instead of returning to the interface region. This effect lowers the amount of vacancies at the interface over repeated cycling with constant write voltage amplitudes, which lowers the interface resistance. It can be corrected by introducing a feedback loop which adjusts voltage amplitudes for the optimal switching ratio during operation [59,60].

State retention over time was tested by applying LRS or HRS state to the device and then measuring the resistance over a timespan of 100 h (Fig. 5b). The HRS and LRS states stay mostly unchanged after the initial relaxation. The resistance drift is small, which is beneficial for the multilevel RS since multiple levels require the device to be stable. The initial relaxation could be beneficial for neuromorphic applications, as it can be used to implement leaky-integrate-and-fire neurons [20].

3.4. Multilevel switching

The dependence of the HRS-resistance on the HRS writing voltage amplitude was used to achieve analog multilevel switching

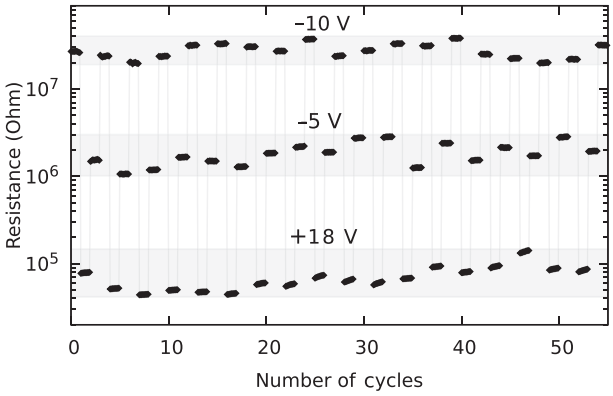

Fig. 7. Demonstration of the multilevel capabilities of the devices. Switching was done by applying constant voltage pulses.

(Fig. 6). In order to do this, we utilized the pulsing protocol depicted in Fig. 6, which consists of several negative writing pulses of different amplitudes and an erase pulse of higher positive amplitude. After each writing (or erasing) pulse we measured the remnant resistance with a small probe voltage of −50 mV which was low enough not to affect the resistive state.

The HRS write amplitude was varied to give rise to multiple different intermediate resistance states spanning from the HRS resistance to the LRS resistance. The applied LRS write placed the device into a known and stable state which worked as a reference point. The remnant resistance (Fig. 6 inset) measured between the writes shows a well-defined dependence to the write amplitude on the negative polarity. As a result, the resistance of the device can be tuned to a desired value between the limiting HRS and LRS resistances. Additionally, multilevel switching was demonstrated with constant amplitude voltage pulses of 100 ms (Fig. 7).

As long as the resistance can be changed in small increments, an error correction algorithm can be used to fine-tune the resistance for improved accuracy [60]. For conventional discrete memory applications, the demonstrated 4 states can be extended by introducing more steps in the writing voltage. The devices are also suited for neuromorphic applications as the switching doesn't have discontinuities in the negative polarity, which allows the storing of synaptic weights [21,22].

4. Conclusions

To summarize, RS devices were manufactured from the perovskite $Pr_{0.6}Ca_{0.4}MnO_3$ with an asymmetric pair of Ag and Al metal interfaces. The devices exhibited stable bipolar switching with multiple intermediate resistive states. The switching was shown to be non-volatile and repeatable. The conduction model analysis indicates an interplay of bulk-limited Poole-Frenkel conduction and interface-limited Schottky conduction depending on the device state, hinting to a modulation of the AlO_x barrier thickness due to field-assisted oxygen vacancy migration. The resistance states show a well-defined dependence on write voltage which allows for a selection of resistance values between two limiting values when a suitable programming sequence is used. The multilevel switching makes the device a candidate for neuromorphic memory applications, although further work is needed in optimizing the devices and taking advantage of their conduction mechanisms in order to better mimic the special functionalities of biological systems.

Acknowledgments

This work was financially supported by the Academy of Finland

project 308285. The authors also acknowledge the Jenny and Antti Wihuri Foundation for financial support. V.L. is also grateful for the support provided by the University of Turku Graduate School.

References

[1] D. Ielmini, Brain-inspired computing with resistive switching memory (RRAM): devices, synapses and neural networks, Microelectron. Eng. 190 (2018) 44–53.
[2] D. Ielmini, H.-S.P. Wong, In-memory computing with resistive switching devices, Nat. Electron. 1 (2018) 333–343.
[3] M.A. Zidan, J.P. Strachan, W.D. Lu, The future of electronics based on memristive systems, Nat. Electron. 1 (2018) 22.
[4] E. Linn, R. Rosezin, S. Tappertzhofen, U. Böttger, R. Waser, Beyond von neumannlogic operations in passive crossbar arrays alongside memory operations, Nanotechnology 23 (2012) 305205.
[5] S. Moradi, R. Manohar, The impact of on-chip communication on memory technologies for neuromorphic systems, J. Phys. D Appl. Phys. 52 (2019), 014003.
[6] W. Maass, Energy-efficient neural network chips approach human recognition capabilities, Proc. Natl. Acad. Sci. U.S.A. 113 (2016) 11387–11389.
[7] K. Kalantar-zadeh, J.Z. Ou, T. Daeneke, A. Mitchell, T. Sasaki, M.S. Fuhrer, Two dimensional and layered transition metal oxides, Appl. Mater. Today 5 (2016) 73–89.
[8] C.-l. Liu, S.-h. Luo, H.-b. Huang, Y.-c. Zhai, Z.-w. Wang, Layered potassium-deficient P2– and P3–type cathode materials KxMnO2 for k–ion batteries, Chem. Eng. J. 356 (2019) 53–59.
[9] F. Bella, A.B. Muoz-Garca, G. Meligrana, A. Lamberti, M. Destro, M. Pavone, C. Gerbaldi, Unveiling the controversial mechanism of reversible na storage in TiO2 nanotube arrays: amorphous versus anatase TiO2, Nano Res. 10 (2017) 2891–2903.
[10] F. Bella, A.B. Muoz-Garca, F. Col, G. Meligrana, A. Lamberti, M. Destro, M. Pavone, C. Gerbaldi, Combined structural, chemometric, and electrochemical investigation of vertically aligned TiO2 nanotubes for Na-ion batteries, ACS Omega 3 (2018) 8440–8450.
[11] S. Galliano, F. Bella, G. Piana, G. Giacona, G. Viscardi, C. Gerbaldi, M. Grtzel, C. Barolo, Finely tuning electrolytes and photoanodes in aqueous solar cells by experimental design, Sol. Energy 163 (2018) 251–255.
[12] T.D. Lee, A.U. Ebong, A review of thin film solar cell technologies and challenges, Renew. Sustain. Energy Rev. 70 (2018) 1286–1297.
[13] F. Bella, A. Verna, C. Gerbaldi, Patterning dye-sensitized solar cell photoanodes through a polymeric approach: a perspective, Mater. Sci. Semicond. Process. 73 (2018) 92–98.
[14] B. Miccoli, V. Cauda, A. Bonanno, A. Sanginario, K. Bejtka, F. Bella, M. Fontana, D. Demarchi, One-dimensional ZnO/gold junction for simultaneous and versatile multisensing measurements, Sci. Rep. 6 (2016) 29763.
[15] S. Bagdzevicius, K. Maas, M. Boudard, M. Burriel, Interface-type resistive switching in perovskite materials, J. Electroceram. 39 (2017) 157–184.
[16] A. Sawa, Resistive switching in transition metal oxides, Mater. Today 11 (2008) 28–36.
[17] X. Hong, D.J. Loy, P.A. Dananjaya, F. Tan, C. Ng, W. Lew, Oxide–based RRAM materials for neuromorphic computing, J. Mater. Sci. 53 (2018) 8720–8746.
[18] P. Stoliar, J. Tranchant, B. Corraze, E. Janod, M.-P. Besland, F. Tesler, M. Rozenberg, L. Cario, A leaky-integrate-and-fire neuron analog realized with a mott insulator, Adv. Funct. Mater. 27 (2017), 1604740.
[19] Y. Pan, T. Wan, H. Du, B. Qu, D. Wang, T.-J. Ha, D. Chu, Mimicking synaptic plasticity and learning behaviours in solution processed SnO2 memristor, J. Alloys Compd. 757 (2018) 496–503.
[20] C. Adda, J. Tranchant, P. Stoliar, B. Corraze, E. Janod, R. Gay, R. Llopis, M. Besland, L.E. Hueso, L. Cario, An artificial neuron founded on resistive switching of Mott insulators, in: 2017 IEEE Int. Mem. Workshop (IMW), 2017, pp. 1–4.
[21] S.H. Jo, T. Chang, I. Ebong, B.B. Bhadviya, P. Mazumder, W. Lu, Nanoscale memristor device as synapse in neuromorphic systems, Nano Lett. 10 (2010) 1297–1301.
[22] K. Moon, A. Fumarola, S. Sidler, J. Jang, P. Narayanan, R.M. Shelby, G.W. Burr, H. Hwang, Bidirectional non–filamentary RRAM as an analog neuromorphic synapse, part i: Al/mo/Pr0.7Ca0.3MnO3 material improvements and device measurements, IEEE J. Electron. Devices Soc. 6 (2018) 146–155.
[23] N. Panwar, U. Ganguly, Variability assessment and mitigation by predictive programming in Pr0.7Ca0.3MnO3 based RRAM, in: 73rd Annu. Dev. Res. Conf. (DRC), 2015, pp. 141–142.
[24] Z. Wang, S. Joshi, S. Savelev, W. Song, R. Midya, Y. Li, M. Rao, P. Yan, S. Asapu, Y. Zhuo, et al., Fully memristive neural networks for pattern classification with unsupervised learning, Nat. Electron. 1 (2018) 137.
[25] D.S. Jeong, C.S. Hwang, Nonvolatile memory materials for neuromorphic intelligent machines, Adv. Mater. 30 (2018) 1704729.
[26] S. Yu, Neuro-inspired Computing Using Resistive Synaptic Devices, Springer International Publishing, 2017.
[27] T.-G. Seong, B.-S. Lee, K.B. Choi, S.-H. Kweon, B.Y. Kim, K. Jung, J.W. Moon, K.J. Lee, K. Hong, S. Nahm, Unipolar resistive switching properties of amorphous $Pr_{0.7}Ca_{0.3}MnO_3$ films grown on a Pt/Ti/SiO_2/Si substrate, Curr. Appl. Phys. 14 (2014) 538–542.
[28] K. Tsubouchi, I. Ohkubo, H. Kumigashira, M. Oshima, Y. Matsumoto, K. Itaka, T. Ohnishi, M. Lippmaa, H. Koinuma, High-throughput characterization of metal electrode performance for electric-field-induced resistance switching in metal/$Pr_{0.7}Ca_{0.3}MnO_3$/metal structures, Adv. Mater. 19 (2007) 1711–1713.
[29] S.-L. Li, J. Li, Y. Zhang, D.-N. Zheng, K. Tsukagoshi, Unipolar resistive switching in high-resistivity $Pr_{0.7}Ca_{0.3}MnO_3$ junctions, Appl. Phys. A 103 (2011) 21–26.
[30] A.M. Sheri, H. Hwang, M. Jeon, B. Lee, Neuromorphic character recognition system with two PCMO memristors as a synapse, IEEE Trans. Ind. Electron. 61 (2014) 2933–2941.
[31] S. Lashkare, S. Chouhan, T. Chavan, A. Bhat, P. Kumbhare, U. Ganguly, PCMO RRAM for integrate-and-fire neuron in spiking neural networks, IEEE Electron. Device Lett. 39 (2018) 484–487.
[32] P. Kumbhare, I. Chakraborty, A. Khanna, U. Ganguly, Memory performance of a simple Pr0.7Ca0.3MnO3-based selectorless RRAM, IEEE Trans. Electron. Dev. 64 (2017) 3967–3970.
[33] X. Liu, K.P. Biju, E.M. Bourim, S. Park, W. Lee, J. Shin, H. Hwang, Low programming voltage resistive switching in reactive metal/polycrystalline Pr0.7Ca0.3MnO3 devices, Solid State Commun. 150 (2010) 2231–2235.
[34] A. Sawa, T. Fujii, M. Kawasaki, Y. Tokura, Hysteretic current–voltage characteristics and resistance switching at a rectifying Ti/$Pr_{0.7}Ca_{0.3}MnO_3$ interface, Appl. Phys. Lett. 85 (2004) 4073–4075.
[35] T. Nakamura, K. Homma, K. Tachibana, Thin film deposition of metal oxides in resistance switching devices: electrode material dependence of resistance switching in manganite films, Nanoscale Res. Lett. 8 (2013) 76.
[36] S. Asanuma, H. Akoh, H. Yamada, A. Sawa, Relationship between resistive switching characteristics and band diagrams of Ti/$Pr_{1-x}Ca_xMnO_3$ junctions, Phys. Rev. B 80 (2009) 235113.
[37] Z.L. Liao, Z.Z. Wang, Y. Meng, Z.Y. Liu, P. Gao, J.L. Gang, H.W. Zhao, X.J. Liang, X.D. Bai, D.M. Chen, Categorization of resistive switching of metal-$Pr_{0.7}Ca_{0.3}MnO_3$-metal devices, Appl. Phys. Lett. 94 (2009) 253503.
[38] M. Fujimoto, H. Koyama, Y. Nishi, T. Suzuki, Resistive switching properties of high crystallinity and low-resistance $Pr_{0.7}Ca_{0.3}MnO_3$ thin film with point-contacted ag electrodes, Appl. Phys. Lett. 91 (2007) 223504.
[39] T. Kramer, M. Scherff, D. Mierwaldt, J. Hoffmann, C. Jooss, Role of oxygen vacancies for resistive switching in noble metal sandwiched Pr0.67Ca0.33MnO3-, Appl. Phys. Lett. 110 (2017) 243502.
[40] P. Kumbhare, I. Chakraborty, A.K. Singh, S. Chouhan, N. Panwar, U. Ganguly, A selectorless RRAM with record memory window and nonlinearity based on trap filled limit mechanism, in: 2015 15th Non–Volatile Mem. Technol. Symp. (NVMTS), 2015, pp. 1–3.
[41] H.-S. Lee, H.-H. Park, The observation of valence band change on resistive switching of epitaxial Pr0.7Ca0.3MnO3 film using removable liquid electrode 107 (2015) 231603.
[42] T. Harada, I. Ohkubo, K. Tsubouchi, H. Kumigashira, T. Ohnishi, M. Lippmaa, Y. Matsumoto, H. Koinuma, M. Oshima, Trap-controlled space-charge-limited current mechanism in resistance switching at Al/$Pr_{0.7}Ca_{0.3}MnO_3$ interface, Appl. Phys. Lett. 92 (2008) 222113.
[43] M.A. Lampert, P. Mark, Current Injection in Solids, Academic Press, 1970.
[44] A. Odagawa, H. Sato, I. Inoue, H. Akoh, M. Kawasaki, Y. Tokura, T. Kanno, H. Adachi, Colossal electroresistance of a $Pr_{0.7}Ca_{0.3}MnO_3$ thin film at room temperature, Phys. Rev. B 70 (2004) 224403.
[45] C. Acha, Graphical analysis of current-voltage characteristics in memristive interfaces, J. Appl. Phys. 121 (2017) 134502.
[46] M. Nyman, T. Elovaara, J. Tikkanen, S. Majumdar, H. Huhtinen, P. Paturi, Epitaxially textured Pr0.6Ca0.4MnO3 thin films under considerably low substrate temperature, Phys. Proced. 75 (2015) 1122–1132.
[47] D.W. Reagor, S.Y. Lee, Y. Li, Q.X. Jia, Work function of the mixed-valent manganese perovskites, J. Appl. Phys. 95 (2004) 7971–7975.
[48] D. Lide, CRC Handbook of Chemistry and Physics, CRC Press I, LLC, 2009.
[49] M.J. Rozenberg, M.J. Snchez, R. Weht, C. Acha, F. Gomez-Marlasca, P. Levy, Mechanism for bipolar resistive switching in transition-metal oxides, Phys. Rev. B 81 (2010) 115101.
[50] T. Kramer, M. Scherff, D. Mierwaldt, J. Hoffmann, C. Jooss, Role of oxygen vacancies for resistive switching in noble metal sandwiched Pr0.67Ca0.33MnO3-δ, Appl. Phys. Lett. 110 (2017) 243502.
[51] N.A. Tulina, A.A. Ivanov, A.N. Rossolenko, I.M. Shmytko, A.M. Ionov, R.N. Mozhchil, S.I. Bozhko, I.Y. Borisenko, V.A. Tulin, X-ray photoelectron spectroscopy studies of electronic structure of Nd2–xCexCuO4–y and YBa2Cu3O7–y epitaxial film surfaces and resistive switchings in high temperature superconductor-based heterostructures, Mater. Lett. 203 (2017) 97–99.
[52] S. Toyoda, T. Namiki, E. Sakai, K. Nakata, M. Oshima, H. Kumigashira, Chemical-state-resolved depth profiles of Al/Pr0.7Ca0.3MnO3 stacked structures for application in resistive switching devices, J. Appl. Phys. 114 (2013) 243711.
[53] E. Dagotto, J. Burgy, A. Moreo, Nanoscale phase separation in colossal magnetoresistance materials: lessons for the cuprates? Solid State Commun. 126 (2003) 9–22.
[54] R. Yang, X.M. Li, W.D. Yu, X.J. Liu, X. Cao, Q. Wang, L.D. Chen, Multiform resistance switching effects in the Al/$La_{0.7}Ca_{0.3}MnO_3$/Pt structure, Electrochem. Solid State Lett. 12 (2009) H281–H283.
[55] D.-J. Seong, M. Hassan, H. Choi, J. Lee, J. Yoon, J.-B. Park, W. Lee, M.-S. Oh, H. Hwang, Resistive-switching characteristics of Al/$Pr_{0.7}Ca_{0.3}MnO_3$ for nonvolatile memory applications, IEEE Electron. Device Lett. 30 (2009) 919–921.
[56] F.-C. Chiu, A review on conduction mechanisms in dielectric films, Adv. Mater.

Sci. Eng. (2014) 1–18, 2014.
[57] W.S. Lau, An extended unified Schottky-poole-frenkel theory to explain the current-voltage characteristics of thin film metal-insulator-metal capacitors with examples for various high-k dielectric materials, ECS J. Solid State Sci. Technol. 1 (2012) N139–N148.
[58] A. Sawa, T. Fujii, M. Kawasaki, Y. Tokura, Interface transport properties and resistance switching in perovskite-oxide heterojunctions, Proc. SPIE 5932 (2005) 59322C.
[59] F. Gomez-Marlasca, N. Ghenzi, P. Stoliar, M.J. Snchez, M.J. Rozenberg, G. Leyva, P. Levy, Asymmetric pulsing for reliable operation of titanium/manganite memristors, Appl. Phys. Lett. 98 (2011) 123502.
[60] P. Stoliar, P. Levy, M. Sánchez, A. Leyva, C. Albornoz, F. Gomez-Marlasca, A. Zanini, C.T. Salazar, N. Ghenzi, M. Rozenberg, Nonvolatile multilevel resistive switching memory cell: a transition metal oxide-based circuit, IEEE Trans. Circuits Syst. II, Exp. Briefs 61 (2014) 21–25.